Unrestricted **EP 2010-5049**

Seismic Monitoring at CO_2SINK: A Feasibility Study

by

J. P. Verdon (EPT-RXX)

Sponsor:	SIEP Rijswijk
Reviewed by:	X. Campman (EPT-RXX)
Approved by:	C. Otto (EPT-RXX)
Date of issue:	March 2010
Period of work:	August - October 2009
Account code:	A-800754-100-01
ECCN number:	Not subject to EAR-No US content

This report documents student work

SHELL INTERNATIONAL EXPLORATION AND PRODUCTION B.V., RIJSWIJK

Further electronic copies can be obtained from the Global EP Library, Rijswijk

SUMMARY

The purpose of this report is to assess the likelihood of CO_2 saturated regions at the CO_2SINK site being detected using a 4-D seismic survey. Some initial work on this subject was conducted by Oates and Garnett (2005; 2006). However, this work assumed that the 80m thick Stuttgart Formation was uniformly and totally saturated with CO_2. In fact, one of the key aspects of the reservoir is that it consists of sandstone channel deposits set in muddier floodplain deposits (Förster 2006). As such, the distribution of channels will be crucial in determining the migration of CO_2. This has already been highlighted with the anomalous (when compared to flow models that do not account for channels) breakthrough of CO_2 at the observation wells. Furthermore, fluid-flow modelling that accounts for the buoyancy of CO_2 in comparison to brine shows that, away from the injection well, CO_2 will not flood the reservoir uniformly, but will rise and spread along the top of the reservoir, forming a thin upper layer whilst the lower parts of the reservoir remain saturated with brine.

Therefore, in this study I aim to reassess the feasibility of detecting thin layers of CO_2 that are migrating through channel deposits. I examine changes to both the reflection amplitudes and travel time shifts. I will consider whether CO_2 plumes can be detected, and whether it is possible to invert seismic observations for CO_2 layer thickness and velocity changes, thereby allowing a volumetric estimate of the amount of CO_2 stored. To do so I will use simple numerical models representing the multiple reflections induced when a plane P-wave travels through a series of closely spaced intervals, as well as full waveform techniques using Shell's in-house finite difference software. In order to compute layer thicknesses and velocity changes, I develop a simple grid-search inversion technique.

I have found a good agreement between simple reflectivity and full waveform modelling, finding that the presence of CO_2 decreases seismic velocities by a sufficient amount to produce detectable amplitude changes. However, the thickness of the CO_2 layers is not sufficient to generate observable travel-time shifts. AVO behaviour is also unaffected by the presence of CO_2. Inversion for layer thickness and velocity change finds a trade-off between these parameters, where thin layers with a high velocity change produce the same 4D amplitude change as a thicker layer with smaller velocity change. Therefore, whilst CO_2 should be detectable with amplitude changes, it may not be possible to make quantitative estimates without additional input from rock physics and/or fluid flow modelling.

As an attachment, in an appendix I discuss the feasibility of using surface deformation to image uplift induced by CO_2 injection using satellite techniques. This modelling is performed using *GEOMEC*.

KEYWORDS

CO_2 storage, Seismic, Monitoring, 4D, Surface deformation

TABLE OF CONTENTS

LIST OF TABLES

LIST OF FIGURES

1. BACKGROUND, VELOCITY MODELS AND 1-D MODELING

1.1. Introduction

Oates and Garnett (2005; 2006) modelled the changes in P-wave velocity (and thereby the reflection coefficients) caused by saturation of the Stuttgart Formation with CO_2. They showed that CO_2 substitution would produce significant velocity changes, and therefore changes in the amplitude of the top-reservoir reflection. Finite-difference waveform modelling suggested that these amplitude changes would be detectable above the noise level. Kazemeini (2009) produced similar work using a velocity model based on sonic logs. This model did include the presence of channels in the Stuttgart Formation, but again it was assumed that the channels were uniformly saturated with CO_2 throughout. I have also identified issues with the velocity models used in both these studies that will be discussed below.

Other CO_2 monitoring projects such as Weyburn (Wilson et al. 2004) and Sleipner (Chadwick et al. 2009) have also shown that the substitution of brine or oil for CO_2 will create easily detectable changes in reflection amplitude. Time-lapse seismic has been less successful at BP's En Salah CCS project, chiefly because there are overlying high impedance layers that prevent much seismic energy reaching the reservoir. It is likely that 4-D seismics will provide a major component of most CCS monitoring programs for the foreseeable future.

Fluid flow models (M. Welling, *pers. comm. 2009)* indicate that buoyancy forces will induce the CO_2 to migrate in thin layers rather than saturating the whole reservoir. Furthermore the presence of sandy channel deposits surrounded by muddy floodplain deposits will strongly influence the CO_2 migration. As such, the Oates and Garnett (2006) block model with 100% saturation throughout the reservoir thickness is not really appropriate. We must instead consider the feasibility of monitoring thin channels containing even thinner layers of CO_2.

The velocity of P-waves in the Stuttgart Formation is approximately $3000ms^{-1}$. For a seismic wave with frequency f=50Hz, the wavelength is λ=60m. The tuning thickness, which identifies the vertical spacing required to identify two separate reflectors is $\lambda/4$=15m. For reflectors spaced closer than this, the reflections will interfere either constructively or destructively depending on the reflection polarization and travel time between reflectors, producing a composite waveform (Kallweit & Wood 1982). The channels in the Stuttgart Formation vary in size, but excepting where channels are stacked on top of each other, they are perhaps 10-30m thick. The layers of CO_2 within such channels will be even thinner. As such, they are below or close to the tuning thickness, and so these tuning effects must be included in the analysis.

The presence of thin layers of CO_2 has an analogy at the Sleipner CCS site, operated by Statoil in the North Sea. Here, thin layers of shale in the Utsira sandstone aquifer trap the CO_2, acting as baffles below which the CO_2 temporarily ponds. Both the layers of shale and the CO_2 saturated layers are thinner than the tuning thickness. However, by constructing composite waveforms based on modelled impedance changes, Arts et al. (2004) were able to forward model the variations in amplitude caused by the thin layers of CO_2, and by comparing these with observations from 4-D seismic, identify the thickness of the CO_2 layers. Ghaderi and Landrø (2009) go a step further by developing an analytical approximation of the tuning effects, and thereby inverting the observed travel-time shifts and amplitude changes directly for both the thickness of the CO_2 layer and the shift in velocity caused by CO_2 substitution. These papers demonstrate that it is possible to not

only identify, but to make quantitative estimates about the properties of, layers of CO_2 saturation that are thinner than the tuning thickness.

1.2. Fresnel Zone

The majority of this work focuses on assessing the vertical resolution of the 4-D survey. However, it is also important to keep in mind the horizontal resolution, given by the width of the first Fresnel zone. This is given by

$$w_f = (2z\lambda)^{1/2}.$$

As an approximation, the Stuttgart Formation is at a depth of 600m, and λ=60m. This gives a Fresnel zone of w_f=270m. Therefore, it will be difficult to reliably identify channels that have a smaller width than this.

1.3. Ray Theory Modelling

In order to model the seismic response, I develop a simple 2-D model consisting of a thin channel of thickness t_{chan}, which contains a layer of CO_2 of thickness t_{CO2}. This is depicted in Figure 1. The plane P-wave, incident at angle θ_i, is reflected from the top of the channel (r_p), from the interface between CO_2 and water in the sandstone (r_{pp1}) and from the base of the channel (r_{pp2}). These three reflections will interfere with each other, producing the composite seismic response. The waves are also refracted as they move through the layers, to an angle of θ_1 in the CO_2 layer and θ_2 in the brine filled sandstone. The initial (pre injection) model has the same features, excepting that the layer of CO_2 is not present, and so we consider the reflections only from mud-sand interfaces at the top and bottom of the channel.

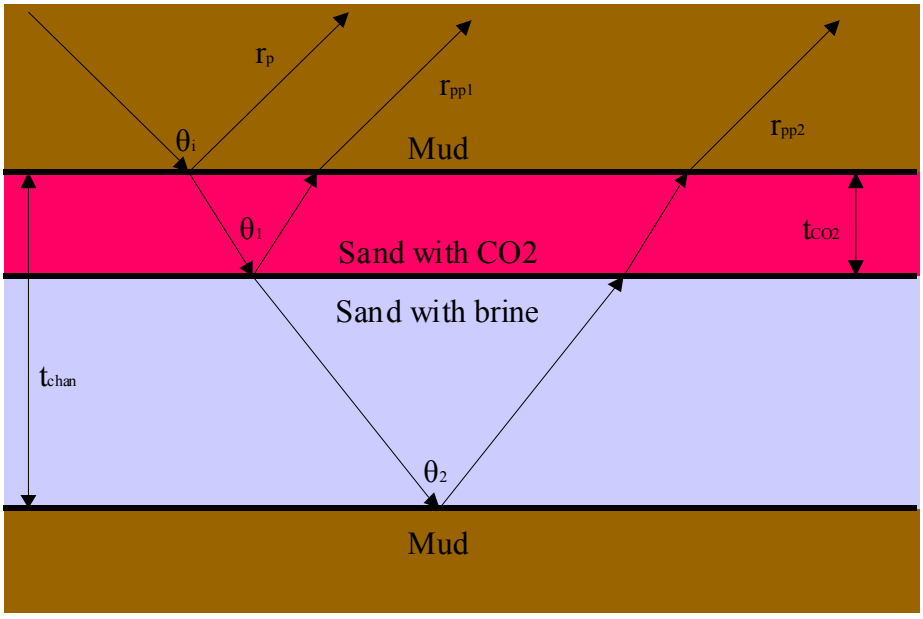

Figure 1: Simple 1-D model used to compute the seismic response for a thin channel that has been partially saturated by CO_2. As tchan<1/4, the response is a composite of reflections from the mud-sand (rp), CO_2-brine (rpp1) and sand-mud (rpp2) interface.

In order to compute the seismic response, I use the equations given by Juhlin & Young (1993), where the response is given as the sum of the reflections produced by the layered model. However, unlike Juhlin & Young (1993), I ignore the contributions from P-S-P

conversions, as these effects were found to be negligible for the models in question. The wave reflected from the top layer is given by

$$r_p(t) = s(t)R_{PP}^{12},$$

where *s(t)* is the amplitude of the incident wave at time *t*, and R^{12}_{pp} is the P-wave reflection coefficient at the mud-CO_2 interface. The wave reflected from the CO_2-water interface will be delayed by an amount

$$d\tau_1 = \frac{2t_{CO2}}{V_{CO2}\cos\theta_1},$$

where V_{CO2} is the P-wave velocity in the CO_2 saturated sandstone. The wave reflected from this layer is given by

$$r_{pp1}(t) = s(t - d\tau_1)R_{PP}^{23}T_{PP}^{12}T_{PP}^{21},$$

where R^{23}_{pp} is the P-wave reflection coefficient at the CO_2-water interface, and T^{12}_{pp} and T^{21}_{pp} are the P-wave transmission coefficients from the mud to the CO_2 layer, and from the CO_2 layer to the mud layer respectively. The P-wave reflecting from the base of the channel is delayed with respect to the CO_2-water reflection by an amount

$$d\tau_2 = \frac{2(t_{chan} - t_{CO2})}{V_{sand}\cos\theta_2},$$

where V_{sand} is the P-wave velocity in the brine-saturated sandstone. The wave reflected from this layer is given by

$$r_{pp2}(t) = s(t - (d\tau_1 + d\tau_2))R_{PP}^{34}T_{PP}^{12}T_{PP}^{23}T_{PP}^{32}T_{PP}^{21},$$

where R^{23}_{pp} is the P-wave reflection coefficient for the base of the reservoir, and T^{23}_{pp} and T^{32}_{pp} are the P-wave transmission coefficients from the water-CO_2 and CO_2-water interfaces respectively. The total reflected waveform is then given by

$$r(t) = r_p(t) + r_{pp1}(t) + r_{pp2}(t).$$

In order to compute the reflection and transmission coefficients at arbitrary incidence angles, I use the linearized Zoeppritz equations given by Ikelle & Amundsen (2005).

There is still some debate as to whether the CO_2-water interface will be of sufficient sharpness to produce a clear reflection. If there is a gradual transition moving spatially from CO_2 saturation to brine, then the seismic velocities will increase gradually, and so there will not be a clear reflection. If the transition is sharp then there will be a sharp change in velocity, and therefore a sharp reflection. Fluid flow modelling has indicated that the transition from significant CO_2 saturation to zero saturation occurs over less than a meter. This would represent a sharp transition capable of generating a reflection. Furthermore, the 4-D seismic changes observed at Sleipner (Arts et al. 2004, Chadwick et al. 2009) are best interpreted as including reflections from CO_2-water interfaces. Therefore I am happy to model them here as a sharp transition.

1.4. Gassmann Substitution

In order to compute the effects of replacement of brine by CO_2 on seismic velocities, I will use the Gassmann substitution equation. This equation describes the change in bulk modulus for a dry rock frame that is saturated by fluids. The saturated bulk modulus is given by

$$K^{sat} = K^{dry} + \frac{\left(1 - \frac{K^{dry}}{K^{m}}\right)^2}{\frac{\phi}{K^{fl}} + \frac{1-\phi}{K^{m}} + \frac{K^{dry}}{(K^{m})^2}},$$

where K^{dry} is the dry frame bulk modulus, K^{m} is the bulk modulus of the minerals that make up the rock frame, K^{fl} is the bulk modulus of the saturating fluid, and ϕ is the porosity. As fluids have no shear strength, the shear modulus of the saturated rock is equal to that of the dry frame, $\mu^{sat}=\mu^{dry}$, and the density is given by

$$\rho^{sat} = \rho^{dry} + \phi\rho^{fl}.$$

The effect of CO_2 substitution on seismic velocities is the subject of much current study. However, uncertainties remain over the exact magnitude of velocity decrease to expect for a given reservoir. This uncertainty arises for a number of reasons: firstly there are a number of models available to compute the effects of saturation change; secondly many of the parameters for these models are difficult to measure; and finally there are other factors as well as saturation change that may influence the velocity change during CO_2 injection.

For example, many authors prefer to use the patchy saturation model or crack-based models rather than Gassmann substitution. When using Gassmann saturation, the dry frame bulk modulus and mineral modulus cannot be measured directly, they must be inferred from measurements on dry cores and/or petrologic analysis. Using the patchy saturation or crack-based models, the patch size or the crack properties are equally as difficult to measure. As well as saturation effects, geochemical reactions may affect the elastic moduli of the rock mass, whilst pore pressure increases during injection will also decrease the velocity (e.g., Verdon et al. 2008). Most lab and field observations of velocity changes with CO_2 saturation predict a P-wave velocity decrease of between 200-600ms^{-1}. The values given by Gassmann substitution for the models discussed below give a velocity decrease of 437ms^{-1}. For the purposes of this work I will go forward with this value, whilst recognizing that further constraints, preferably based on experimental measurements, would be preferred.

1.5. Velocity Model for Ketzin Reservoir

In order to simulate the seismic response, the velocities and densities of the layers in question must be known. Velocities are usually modelled using a blocked velocity model based on borehole sonic velocity logs and/or seismic data. Both Oates and Garnett (2006) and Kazemeini (2009) have constructed velocity models for Ketzin. These models both have significant impedance contrasts at the top of the reservoir. These create an easily observable reflection when 1-D elastic (Kazemeini 2009) or 2-D finite difference waveform modelling (Oates & Garnett 2006; Kazemeini 2009) techniques are used to simulate reflections from the reservoir.

In reality, for the baseline 3-D survey no clear reflection was observed from the top of the Stuttgart Formation (Juhlin et al. 2007). Only by amplitude summation across the anticipated time interval was a weak signal detected for the Stuttgart Formation. The results from a cross-line of the baseline 2006 survey are plotted in Figure 2 (Juhlin et al. 2007). This discrepancy – between a baseline survey where no strong reservoir reflection was identified, and synthetic modelling that produces strong baseline reflections – is important because both Kazemeini (2009) and Oates & Garnett (2006) have asked the question 'can

changes to an already observable reflector be detected?', when in fact the pertinent question is 'will a presently unreflective layer be made detectable by the presence of CO_2?'.

The sonic log from observation well Ktzi-202 is plotted in Figure 3a. The figure is dominated by the presence of the anhydrite at the top of the Weser Formation. In Figure 3b I provide a closer look at the reservoir level (the top of the Stuttgart Formation is at 630m here). There is a fairly clear decrease in P-wave velocity at the top of the reservoir, which must be accounted for in our modelling. In Figure 3c I plot the density log at reservoir depths.

It is known that the sand body into which CO_2 is being injected is approximately 20m thick. This is close to the tuning distance for P-waves at reservoir depth. If two reflectors, separated by the tuning distance, have opposite polarities then they will interfere constructively, producing an even larger reflection signal. If, however, they have the same polarity then they will interfere destructively, reducing the magnitude of the reflection (Kallweit & Wood, 1982). A model velocity that generates reflections of the same polarity from the top and base of the Stuttgart sand channel is not unreasonable when compared with sonic log data from the reservoir level (Figure 3b). The full velocity model that I have developed, based on the sonic log information in Figure 3a, is described in Table 1 and plotted in Figure 3. In Figure 4 I compare my updated velocity model with those of Oates & Garnett (2006) and Kazemeini (2009).

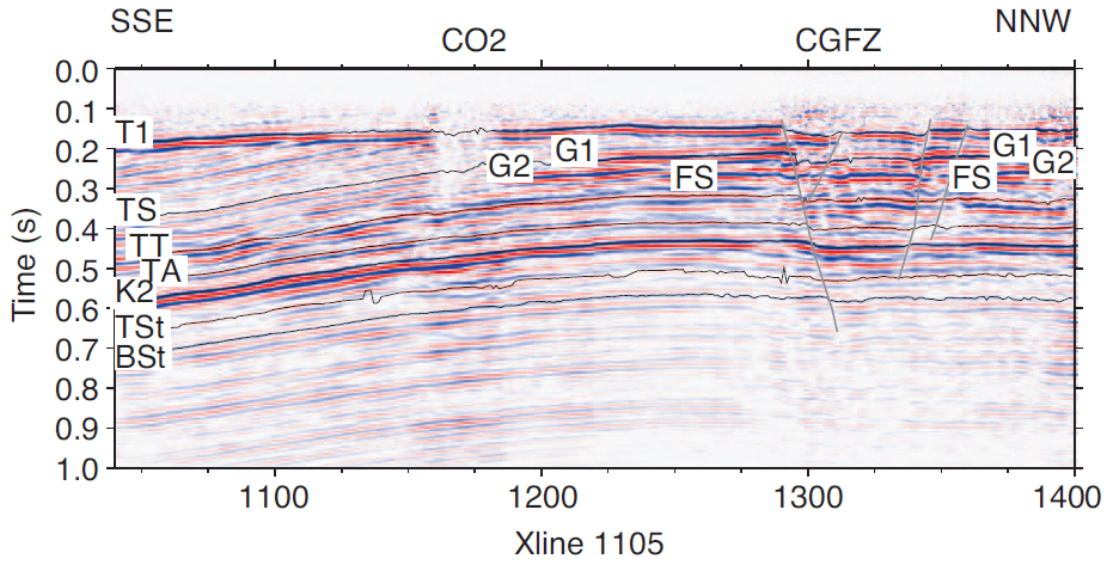

Figure 2: **Results from the baseline seismic survey (from Juhlin et al. 2007). The anhydrite layer produces a clear reflection (K2). There are only weak reflections from the reservoir layer (TSt).**

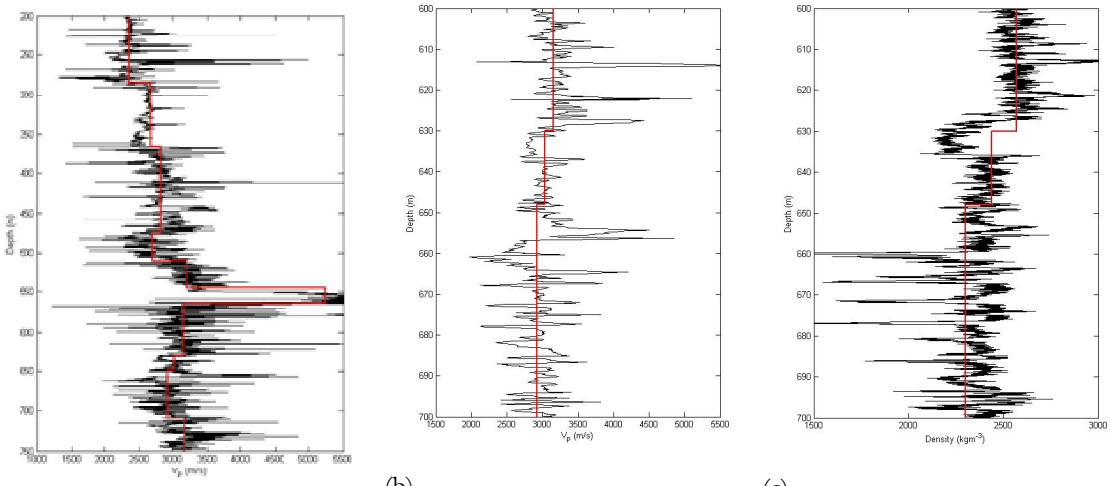

Figure 3: **Sonic log (black) and my blocked velocity model (red) for the Ketzin rocks. In (a) I show the whole system, whilst in (b) I focus on the Stuttgart Formation (at a depth of 630m). In (c) I show the density log over the reservoir interval.**

Table 1: **Proposed velocity model for the Ketzin reservoir.**

Layer	Depth to top (m)	P-wave velocity (ms^{-1})	Density (kgm^{-3})
1	0	2350	1950
2	285	2660	1950
3	365	2825	2140
4	475	2680	2250
5	510	3200	2340
6	545	5250	2700
7	565	3150	2570
8	630	3030	2440
9	648	2920	2300
10	710	3170	2640

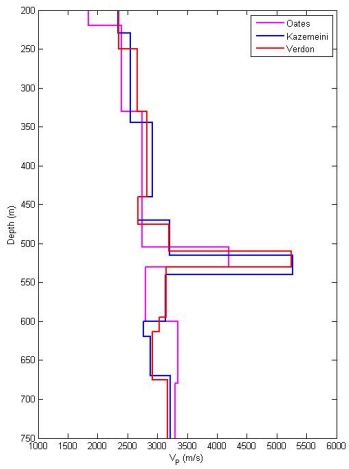

Figure 4: **Velocity models used by the 3 authors (Oates & Garnett (2006), Kazemeini (2009), and this work. All share many similarities, particularly in and above the stiff anhydrite layer.**

I use simple reflectivity modelling as a quick way of examining the seismic response. In essence, this is achieved by convolving a source wavelet – in this case a Ricker wavelet with a dominant frequency of 50Hz – with the reflection profile. In Figure 5 I plot the seismic response from the reservoir layer using this method for all 3 velocity models (Oates & Garnett 2006, Kazemeini 2009, this study). I find that the reflection from the top of the Stuttgart Formation using the updated model is much reduced in comparison with the earlier models, providing a much closer approximation of what has been observed in the real seismic data from Ketzin.

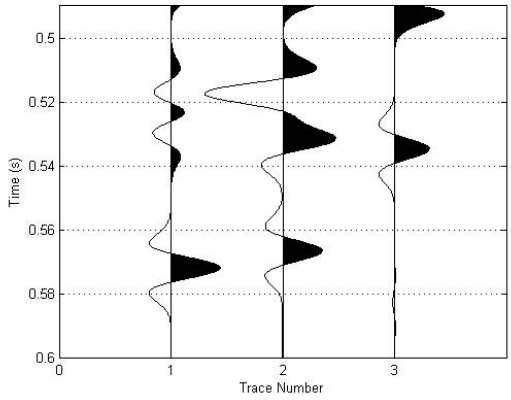

Figure 5: **Seismic response for a normal incidence wavelet reflected from the reservoir level for all three Ketzin velocity models. Trace 1 is this work, trace 2 is Kazemeini (2009) and trace 3 is Oates & Garnett (2006). The top reservoir reflection is at ~0.51s TWTT. The reflections from the velocity model presented in this study are smaller in amplitude than those from the previous Ketzin velocity models.**

Normally distributed white noise is added to the trace, and in Figure 6 I plot the noisy trace produced by the updated velocity model. The reflection from the top of the reservoir is barely observable above the noise level. This is a far more accurate representation of the observed seismic data (Figure 2) than either of the earlier proposed velocity models.

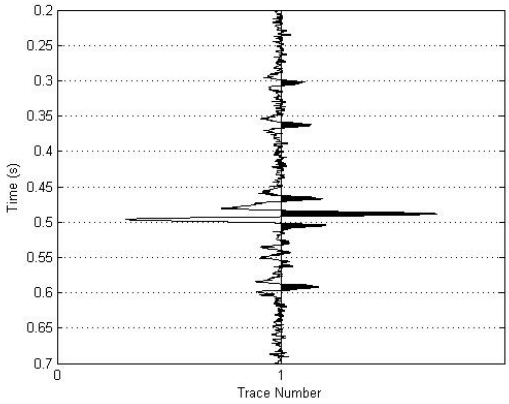

Figure 6: **Seismic response for the updated velocity model, with artificial noise added. The response from the reservoir level (at ~0.52s TWTT) is barely observable above the noise. This provides a better match with the observed seismic data (Figure 2) than either of the earlier proposed velocity models.**

For the subsequent modelling I consider the velocity model generated here as well as, in Model B, the models of Kazemeini (2009), and in Model C, the Oates & Garnett (2006) model. The velocities and densities are given in Table 2. It is likely that the sand channels in the formation are of variable thickness, and that the thickness of the CO_2 layer is also variable. I test models with t_{chan} in the range [10,40] and t_{CO2} in the range [1,5]. The six models that I consider are described in Table 2. There are also a number of parameters that will remain invariant throughout this modelling. These parameters are given in Table 3.

Table 2: **Description of the physical parameters that are varied between the 6 models considered here. The variables are, from left, P-wave velocity in the overlying Weser Formation, P-wave velocity in the brine saturated Stuttgart channel deposits, P-wave velocity in the Stuttgart floodplain deposits, the densities of these three formations, the thickness of the channel, and the thickness of the CO_2 layer within the channel.**

	V_P^W (ms^{-1})	V_P^S (ms^{-1})	V_P^u (ms^{-1})	ρ^W (kgm^{-3})	ρ^S(kgm^{-3})	ρ^u(kgm^{-3})	t_{chan} (m)	t_{CO2} (m)
A	3150	3030	2920	2570	2440	2300	20	5
B	3140	2765	2880	2560	2070	2470	20	5
C	2800	3350	3300	2440	2383	2400	20	5
D	3150	3030	2920	2570	2440	2300	40	5
E	3150	3030	2920	2570	2440	2300	10	5
F	3150	3030	2920	2570	2440	2300	20	1

Table 3: **Physical parameters that are not varied in the construction of the following models.**

Parameter	Description	Value
ϕ	Channel porosity	0.2
K^b	Brine bulk modulus	3 Gpa
K^{CO2}	CO_2 bulk modulus	0.02 Gpa
K^m	Channel mineral bulk modulus	33 Gpa
ρ^b	Brine density	1150 kgm^{-3}
ρ^{CO2}	CO_2 density	700 kgm^{-3}
F	Frequency of incident wave	50 Hz
V_P:V_S	P- to S-wave ratio	1.7
S_g	Saturation of CO_2 in gas layer	0.15

1.6. Results

In Figure 2 I show the seismic response of each model before and after saturation by CO_2. Each trace is at an incidence angle of θ_i=5°. As well as the overall response, I show the contributions from each reflection. I will discuss the change in amplitude of the signal (dA), the travel-time shift calculated by cross-correlating the waveforms before and after, and finding the time shift that maximizes this value (dt'). I will also consider the time shift that would affect a wave reflecting from a layer below the Stuttgart Formation (dt). As can be seen, the introduction of a CO_2-water reflection and the change from brine to CO_2 saturation at the top-channel reflection serves to increase the reflection amplitude in most cases. The AVO behaviour is plotted in Figure 8. For all the models where the CO_2 layer is 5m thick, an increase in amplitude is observed. This is significant, because it may mean that reflections that were previously below the noise level may become visible. However, whilst the AVO behaviour is different between the models, the introduction of CO_2 does not significantly change the AVO behaviour of any of the models. This suggests that AVO may not be a useful tool for indicating the presence of CO_2. For the model with a layer of CO_2 only 1m thick (model F), the change in amplitude induced by the presence of CO_2 is not of an appreciable magnitude. This suggests that CO_2 layers this thin may not be detectable. The difference in amplitude before and after CO_2 substitution is also plotted. I note that the largest amplitude changes are generally found at incidence angles of ~10°.

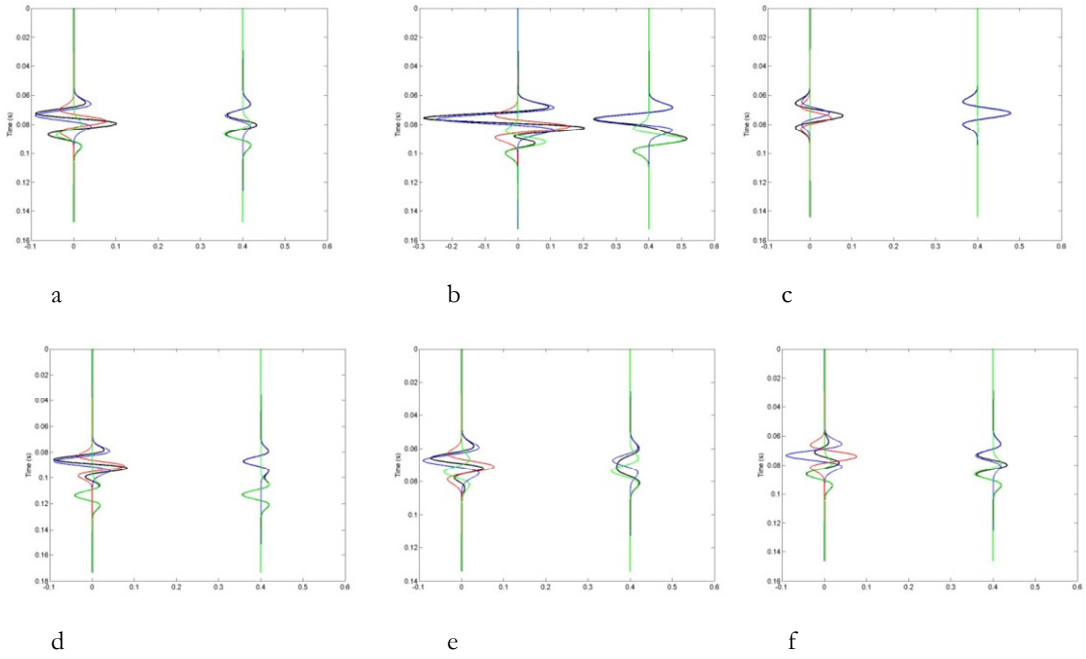

Figure 7: **Response for a wave incident at 5° for the 6 models (a)-(f), showing the response before (right-hand traces) and after (left-hand traces) CO_2 injection. As well as the total response (black), I show the individual contributions from the top-channel (blue), base-channel (green) and CO_2-water interface (red) reflections.**

The time shifts caused by the presence of CO_2 are plotted in Figure 9. I plot the time shifts that would be experienced by a reflection from a lower layer as well as the apparent time shift computed by cross-correlating the responses. The response from the cross correlation is complicated, highly non-linear and often quite large. This is because the introduction of a reflection from the CO_2-water interface, and the resulting interference, can change the shape of the reflected response, making the cross-correlation technique unreliable. The

time shifts experienced by a reflection from an arbitrary layer below the Stuttgart Formation are also plotted in Figure 9. These are much easier to interpret, as they simply represent the additional travel time introduced by a wave having to through the slower CO_2 layer. The time shifts induced in this manner are small, excepting for the Kazemeini (2009) velocity model (B). Given that the sampling rate of the geophones used at Ketzin is 1ms, it will be difficult to detect time shifts of this order – the layers of CO_2 are simply not thick enough for an appreciable time shift to accumulate. This is an analogous to the Weyburn CCS monitoring program, which found that the reservoir was too thin (30m) for observable time shifts to develop (Wilson 2004). Instead, only changes in amplitude can be used to identify zones of CO_2 saturation.

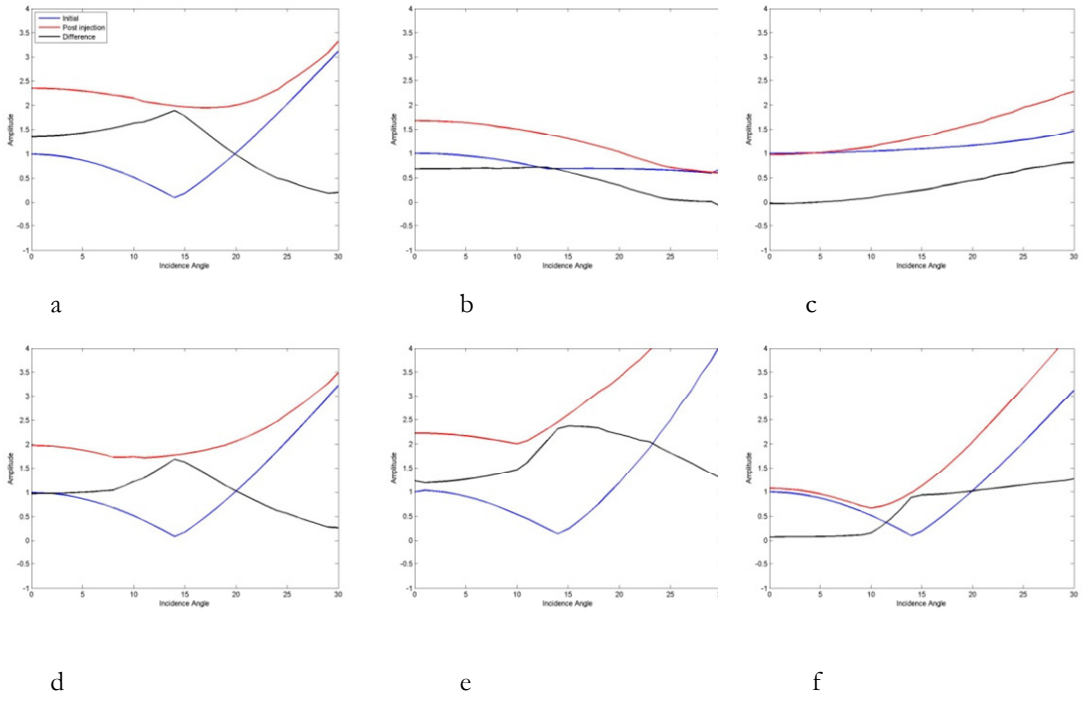

Figure 8: **AVO response for the 6 models (a)-(f), showing the amplitude of reflection as a function of incidence angle before (blue) and after (red) CO_2 injection, and the difference between them (black). All values are normalized by the amplitude of the zero offset reflection before CO_2 saturation. In most cases, the reflection amplitude is increased by the presence of CO_2, although the AVO behaviour is essentially unchanged.**

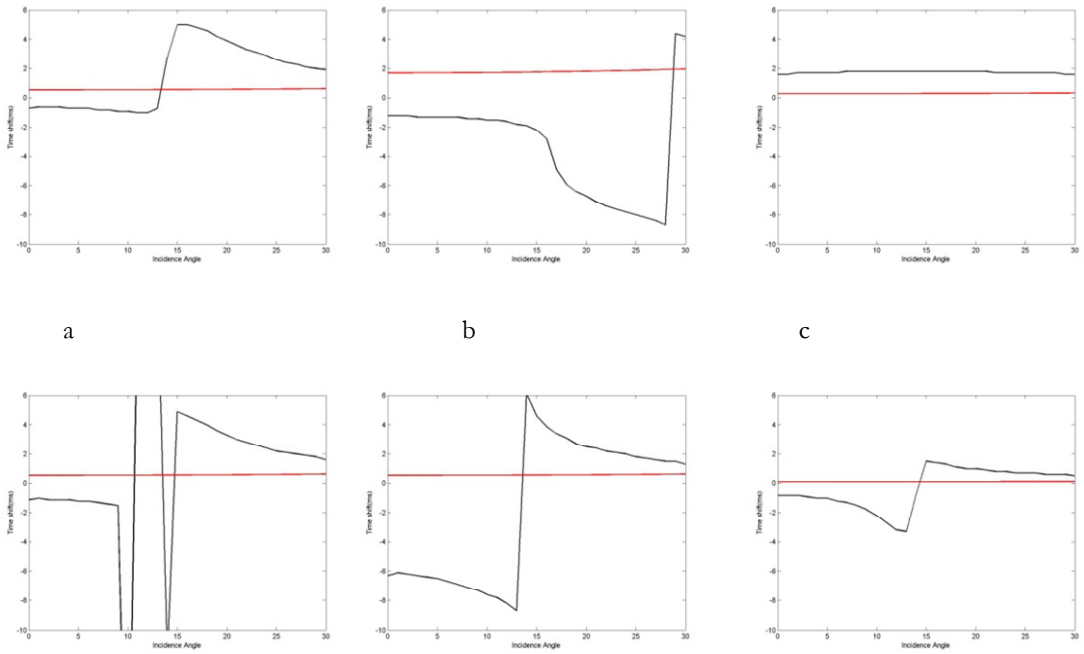

Figure 9: Actual time shifts (red) experienced by reflections from below the reservoir, and the apparent time shifts cross-correlating the reservoir reflection (black) as a function of incidence angle for the 6 models (a)-(f).

To summarize, these models suggest that regardless of the relative velocities and thicknesses of the mud and sand layers, the changes in velocity induced by substitution of brine by CO_2 are large enough to create increases in the amplitude of the reflected wave. Therefore, in time-lapse surveys this parameter must be considered as the primary indicator for the presence of channels filled with CO_2. Time shifts, and changes in AVO behaviour seem to be less promising as indicators of CO_2 saturated layers.

1.7. Quantitative Estimates Using Time-Lapse Seismics

It is possible to use 4-D seismic observations to make quantitative estimates for the thickness and velocity of a thin CO_2 layer. Both the changes in travel-time (*dt*) and reflection amplitude (*dA*) are mutually dependent the layer thickness and velocity. Therefore, the layer properties can, in theory, be inverted from the seismic observations *dt* and *dA*. This inversion has been conducted for the thin CO_2 layers at Sleipner by Ghaderi and Landrø (2009). They make several approximations in order to develop an analytical relationship (an inverse sinc function) between the changes to the reflection amplitude and time shift with changes to the layer thickness and velocity using a 3-layer model (sand with brine, sand with CO_2, sand with brine). I am reluctant to make the approximations used by Ghaderi and Landrø (2009) unless necessary, and the model for the Stuttgart Formation is also more complex, with 4 layers instead of 3 (floodplain, channel with CO_2, channel with brine, floodplain). Therefore I have instead developed a numerical approach to solve this problem. As well as removing the need to make certain approximations, this has the advantage of determining how well constrained the result is. This is crucial because the seismic response is often highly non-unique, with many combinations of (quite different) CO_2 layer thicknesses and velocity changes giving similar seismic responses. However, this approach is more computationally expensive, taking between 60-360 seconds to run on a desktop computer.

In order to conduct the inversion, I first generate the 'observed' data using the forward models discussed above. To invert the observed data, I compute the time shifts and amplitude changes for a range of velocity changes (dV) and CO_2 layer thicknesses (t_{CO2}). The model that minimizes the misfit between itself and the 'observed' value is taken as being the most appropriate. By plotting the misfit contours over the range of dV and t_{CO2}, I can determine how well constrained the inversion is. Because of the strongly non-linear response of the apparent time shifts measured with cross-correlation (dt'), I consider here the time shifts experienced by deeper reflectors (dt).

In Figure 10 I forward model the changes in amplitude (dA) and time shifts (dt) caused by the presence of a layer of CO_2 with thickness t_{CO2} and velocity reduction dV. The thickness of the channel and the initial sand and mud velocities are assumed as known. The 'observed' dt and dA values based on the models presented above are marked by red '+'s. I minimize the misfit to determine which of the calculated lines best fits the observed seismic response. The misfit contours as a function of dV and t_{CO2} are plotted in Figure 11 for each model. It can be clearly seen that in no case is the solution well constrained – there is always a range of dV and t_{CO2} values that could fit the observation. This can also be understood from Figure 10, where many of the calculated lines go through or near the red '+' marking the observed value.

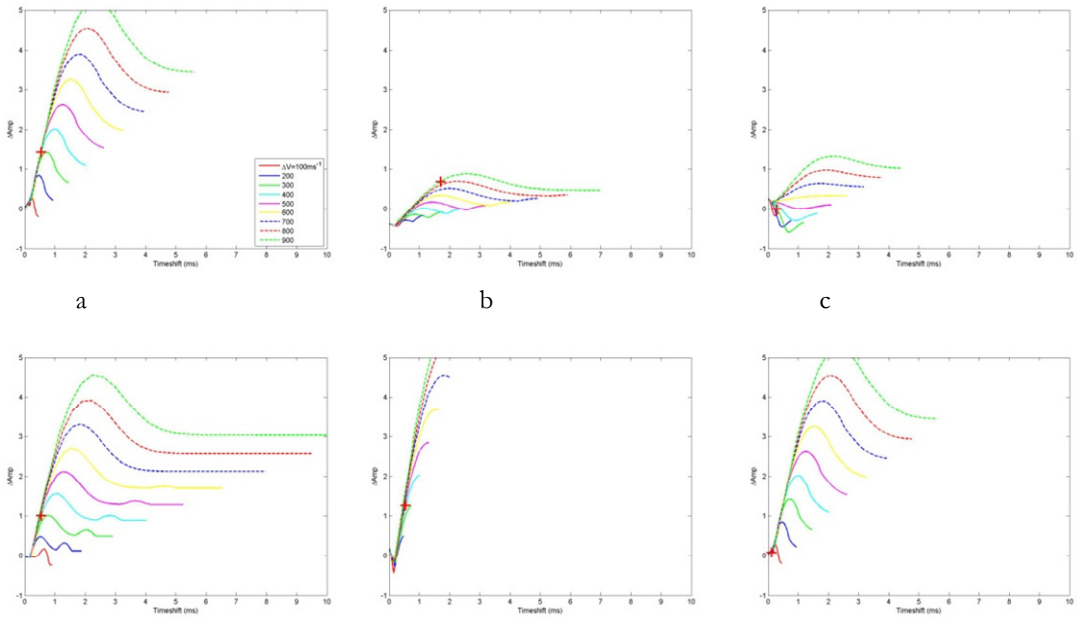

Figure 10: **Forward modelling for the time shifts and amplitude changes for a range of models with varying thickness and velocity change. The red '+' marks the modelled result for the model in question (a)-(f). It is clear that in all cases a range of dV and t_{CO2} will give the same response in terms of amplitude and time shifts.**

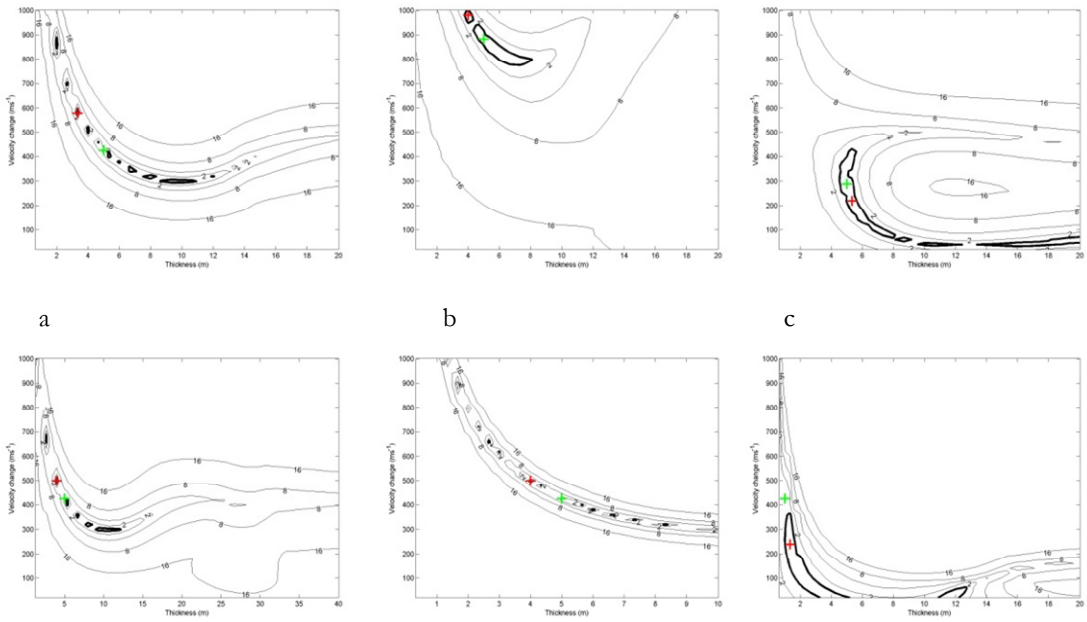

Figure 11: **Contours showing the misfit of amplitude and time shift as a function of model t_{CO2} and dV. Contours are normalized such that 1 represents the 90% confidence interval. The minimum misfit value is marked by a red '+'. The green '+' marks the input values for the model. Note the trade off between t_{CO2} and dV means that the best-fit result is rarely well constrained.**

It is notable that not a single of the models presented above produces a change in amplitude and time shift that could be reliably and uniquely inverted for layer thickness and velocity change. Note also that this inversion method assumes that the initial velocities and the channel thickness are known (and the correct values are used), and does not add noise to the original, forward modelled data. At best I find a trade-off between the t_{CO2} and dV parameters. This suggests that quantitative inversions will be difficult to conduct on future Ketzin seismic data. However, if rock physics models could be developed that reliably constrain probable values of dV, thickness of the CO_2 layer to be computed from the changes in amplitude.

Having modelled the seismic response using simple reflectivity modelling, I will now go on to model the response using full waveform simulation. By using the full wave-field and including the effects of multiples and wave conversions, this will provide a more complete approximation of the response to CO_2 injection at Ketzin.

2. FULL WAVEFORM MODELING

2.1. Introduction

To further test the inferences that I make in the first part of this report, I now examine the same models using full waveform finite difference simulation. I use Shell's in-house *wfd* package. A 2-D model is developed, with a width of 1400m and a maximum depth of 800m. I use the same velocity model as described in the previous section. A vertical force at the surface is used as the source, corresponding to the weight-drops used at CO_2SINK. The model is depicted in Figure 12, and described in Table 4. CO_2 substitution was modelled as a continuous layer with constant thickness (to be varied between models) and a 400ms^{-1} velocity decrease. The upper surface was treated as a free surface, and damping layers were added to the edges of the model to remove unwanted edge reflections. The receiver geometry – 25m spacing and a maximum offset of 700m – is a 2-D representation of the receiver pattern used in the baseline CO_2SINK survey. Synthetic seismic traces were generated for vertical motion at each receiver, and an example of a typical shot gather is plotted in Figure 13.

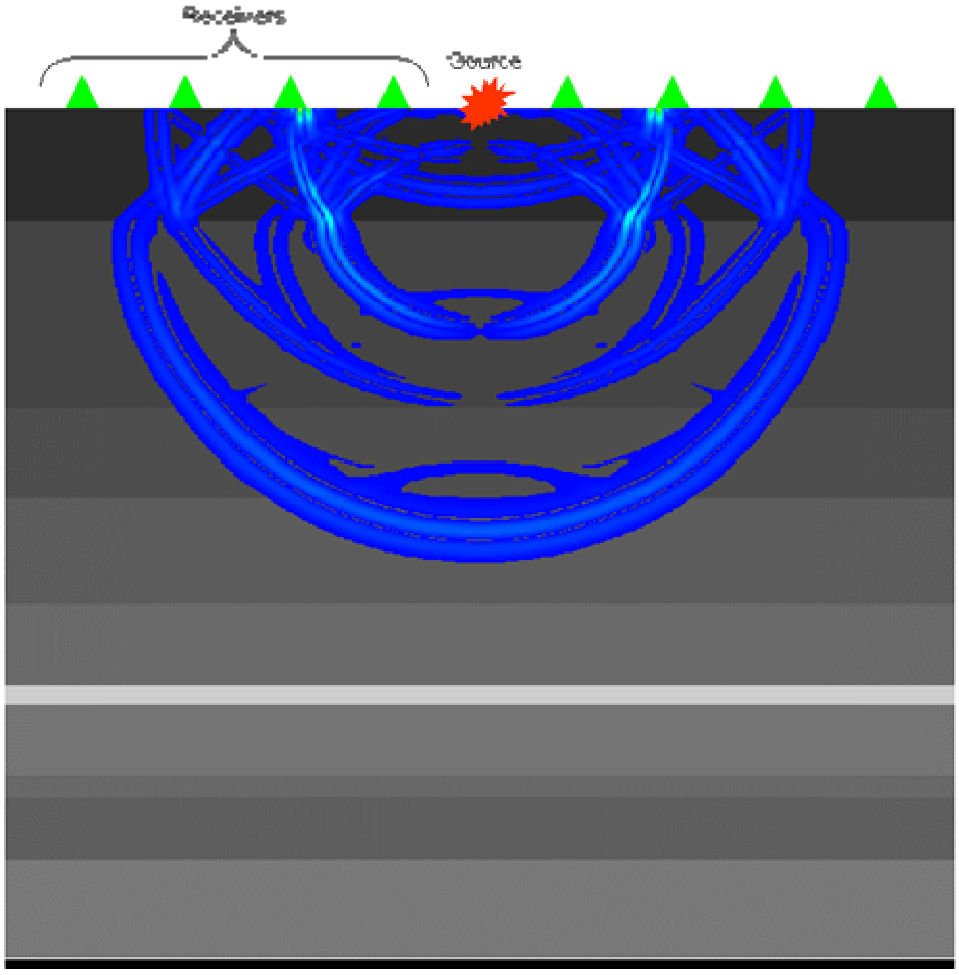

Figure 12: **Annotated snapshot showing a cross-section of the full waveform modelling setup. The source is located at the surface in the center of the model, with receivers placed to either side. The shades of grey indicate the impedances of the layers, with the highest impedance (nearly white) representing the anhydrite layer.**

Table 4: Model parameters used for finite difference waveform modelling. Three models are developed with differing thickness of CO_2.

Parameter	Model Value
Model Dimensions	1400X800m
Source location coordinates	700X0m
Number of receiver	56
Receiver spacing	25m
Computational grid spacing	2X2m
Source wavelet	Ricker
Source frequency	50Hz
Solution method	Elastic
CO_2 layer thickness	[2,5,10]m

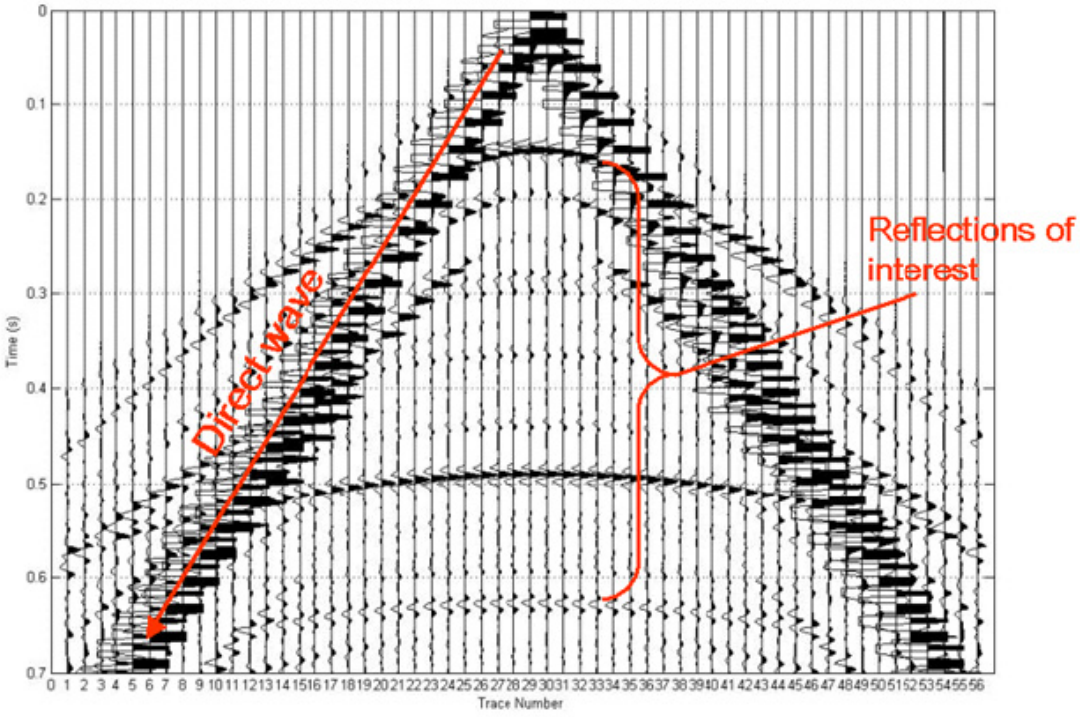

Figure 13: Example of raw shot data generated by finite difference simulation. The direct wave and the reflections from the subsurface are marked.

A very strong direct wave (ground-roll) is found across all the traces – this is removed by muting. An example of the shot gather after the mute function has been applied is shown in Figure 14. For the low-offset traces, the reservoir reflections arrive long after the direct wave, whilst at larger offsets they become coincident. Therefore, in the subsequent analyses I consider only traces with a small enough offset such that the reflections of interest are not overwhelmed by the large amplitude surface waves. The strongest body-wave reflection comes, as expected, from the anhydrite layer. Note also a near-surface multiple of this reflection arriving ~0.1 seconds after the primary arrival, where the arrival reflects from the free surface and then returns from the relatively strong, near surface Base-Tertiary reflector

(T1). This multiple arrives close to the arrival of a genuine reflection from the reservoir, and it is important to avoid confusing the two when processing the data. It is possible that this multiple is present in the baseline surface data as well – it would be expected in the vicinity of arrival BSt (in Figure 2), but without access to the real data this is only speculation.

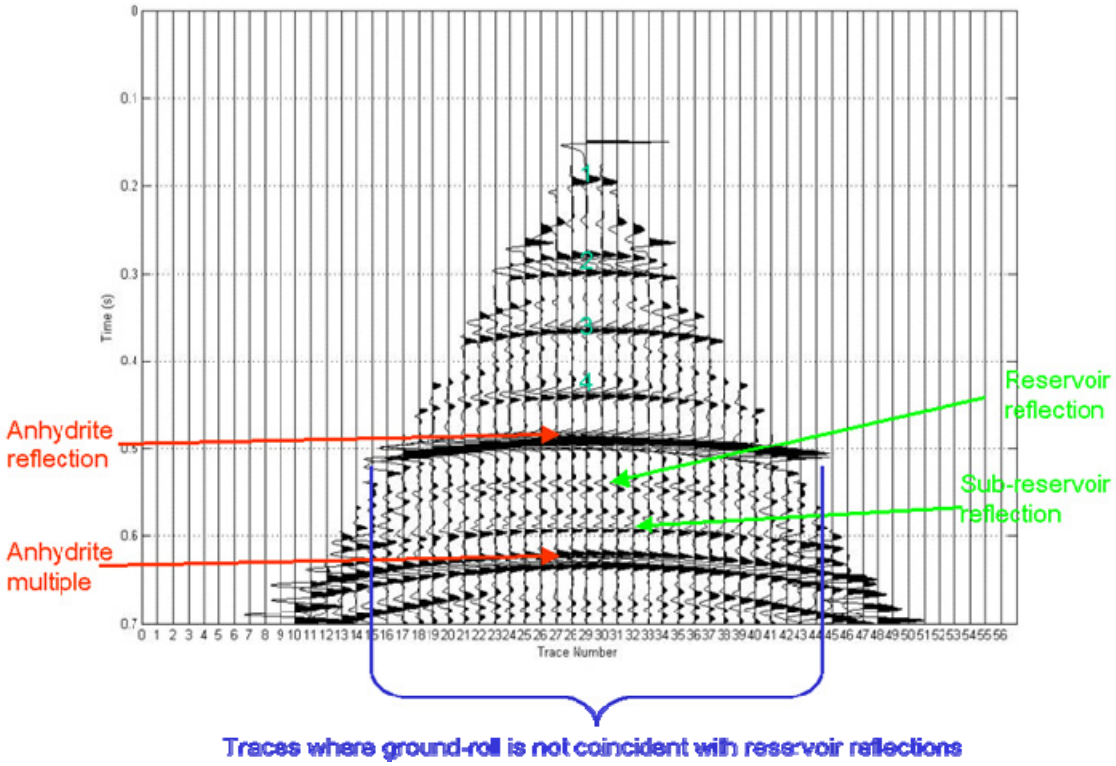

Figure 14: **Shot gather with direct waves removed. The reflection and multiple from the anhydrite, the reflection from the reservoir and the reflection from below the reservoir are all marked. The reflections in the overburden correspond to (1) T1, (2) TS, (3) TT, and (4) TA from Figure 2.**

2.2. Data Processing

The first stage in data processing was the removal of the direct wave using a mute function. Where the reservoir reflections are coincident with the direct wave, they are also removed by the mute. Therefore, these traces are discarded. The arrivals from the reservoir and from the reflector below the reservoir are picked on the zero-offset trace, and the normal moveout curves computed using the rms velocities. The normal moveout curves provide virtual picks, allowing all the arrivals excepting that from the reservoir and sub-reservoir reflectors to be discarded with a taper. Changes in travel time are computed by finding the maximum cross-correlation between the sub-reservoir reflectors before and after CO_2 substitutions, whilst amplitude changes are computed using the difference between the maximum amplitudes found over the reservoir interval.

2.3. Results

I begin by considering time shifts for the sub-reservoir reflection. These are plotted in Figure 15 as a function of incidence angle at the reservoir. In Figure 15(a) I plot the time shift for a model where the CO_2 layer is 5m thick, and the receiver sampling rate is 1ms. No time shifts are detected – this is because the anticipated time shifts are less than the sampling rate. With a faster sampling rate of 0.1ms (Figure 15(b)), the changes in travel

time can now be detected. Unfortunately, the geophones at CO_2SINK only sample at 1ms, so I do not anticipate detectable time shifts. Figure 15(c) and Figure 15(d) show the time shifts for CO_2 layers of 2m and 10m thick respectively, with a 0.1ms sampling rate. The time shifts for the 2m layer are even smaller than for the 5m layer, whilst the time shifts for the 10m thick layer are of the order 1ms. This would be detectable with a 1ms sampling rate, but not with any kind of resolution.

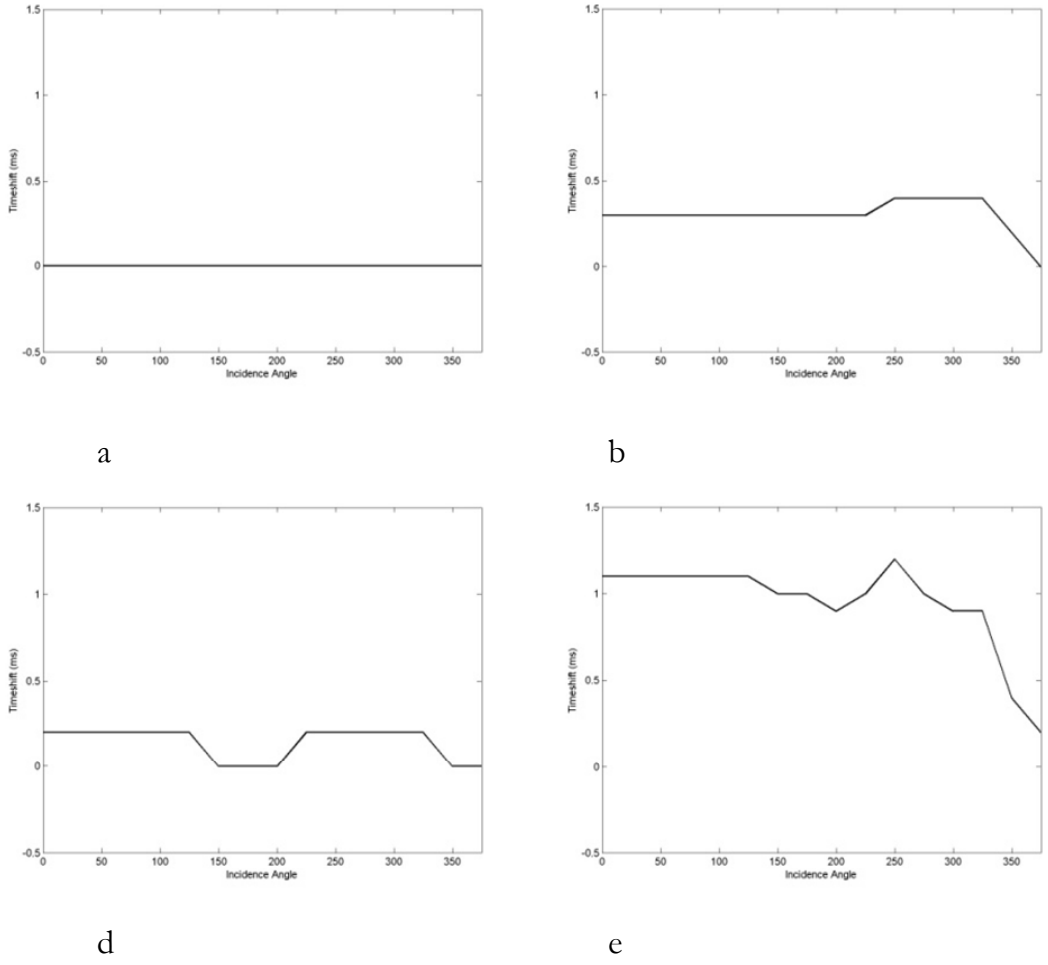

Figure 15: **Time shifts from the sub-reservoir reflector, with a layer of CO_2 of thickness 5m (a) and (b), 2m (c), and 10m (d). In (a) the sampling rate is 1ms, so no change is detectable. In (b), (c) and (d) the sampling rate is 0.1ms, making the time shifts detectable.**

The changes in amplitude for the 5m, 2m and 10m thick layers are plotted in Figure 16. The amplitudes are normalized to the pre-injection zero-offset amplitude. These curves resemble, albeit noisily, the results from the earlier modelling conducted above. As with the ray-based modelling, the AVO behaviour does not alter significantly with the presence of CO_2. The amplitude increases are found to be largest at small offsets, and larger for thicker layers of CO_2. This implies that there will be a minimum thickness of CO_2, below which amplitude changes will not be identifiable. The largest amplitudes are at larger offsets both before and after CO_2 substitution. However, at larger offsets the amplitude is less sensitive to fluid substitution.

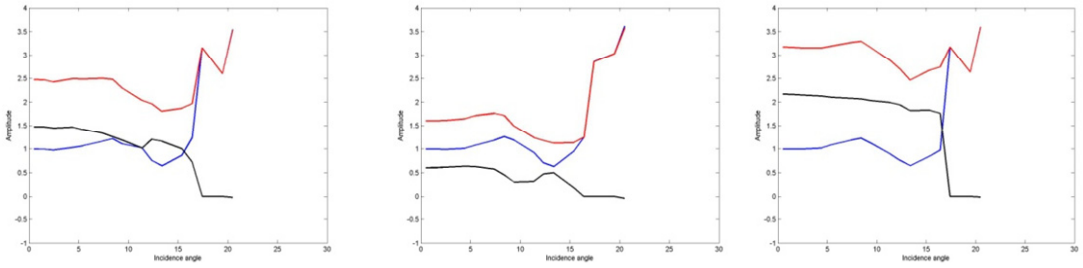

a b c

Figure 16: Reflection amplitudes before and after CO_2 substitution, and the time-lapse difference, for models with (a) 5m, (b) 2m and (c) 10m thick CO_2 layers. Amplitudes are normalized relative to the amplitude of the zero-offset trace before CO_2 substitution

2.4. Quantitative Estimates Using Time-Lapse Seismics

In this section I use the inversion method described previously to invert the full waveform modelling data for the layer thickness and velocity change. For each model I use all the traces, stacking the misfit surfaces to find the value(s) that best fit all of the traces combined. The results for the 4 models are plotted in Figure 17. The initial parameters are marked by a green +, the results by a red +. A successful inversion will find these to points to be similar. In all cases, the trade-off between velocity change and layer thickness is apparent, even when the results from 30 receivers are stacked. In some cases the trade-off is less constrained than others. The model with a 1ms sampling rate is shown in Figure 17(a). As discussed above, the sampling rate is not sufficient to resolve the time shift, and so the inversion struggles to find the 'correct' answer. For model C, with a 2m thick layer, the amplitude changes and time shifts are both very small, so the inversion again struggles. Only Model D, with a 0.1ms sampling rate and 10m layer thicknesses, finds the 'correct' answer. However, the 'trough' of plausible values is again apparent, ranging from thin layers with a high velocity shift to thick layers with a small velocity shift. The trade-off identified with the simple ray-based modelling is present when we move to full waveform modelling as well.

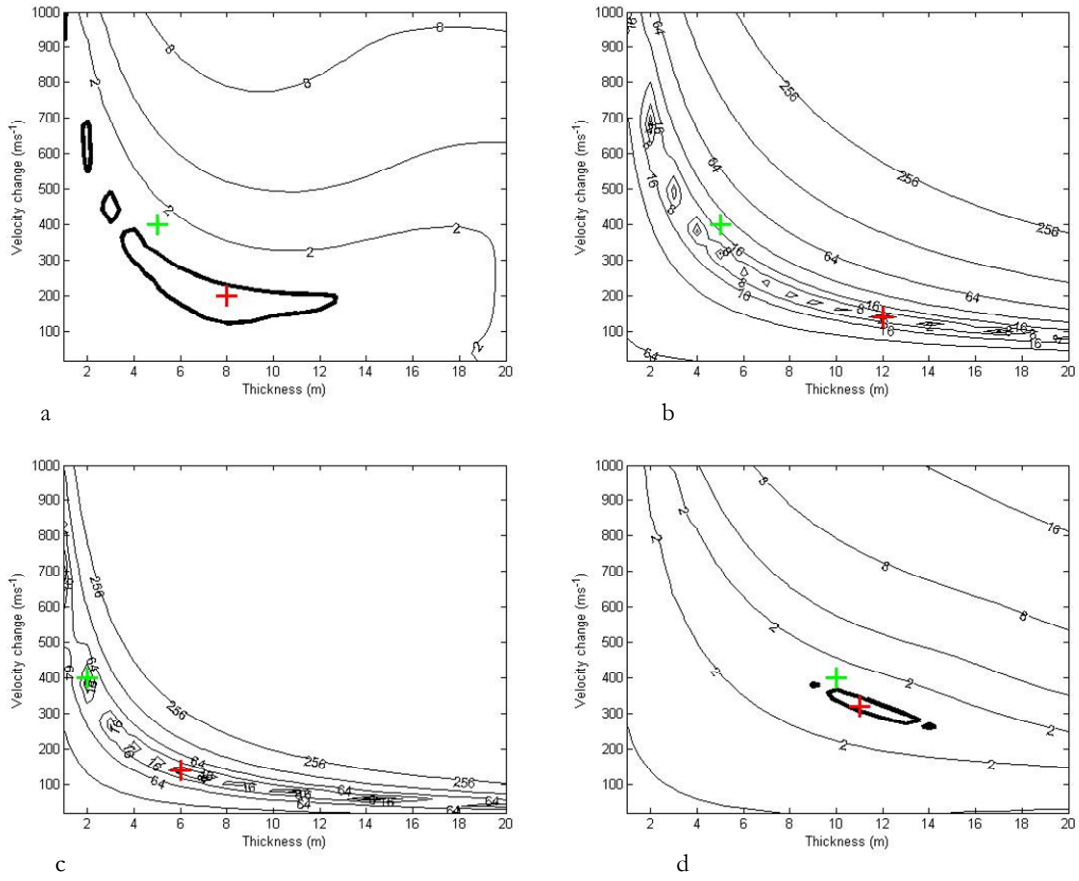

Figure 17: **Results for the inversion of time lapse observations for CO_2 layer thickness and velocity change. Model (a) has a CO_2 layer 5m thick and a 1ms sampling rate. Models (b), (c), and (d) have thicknesses of 5m, 2m and 10m respectively, and sampling rates of 0.1ms.The best-fit inversion result is marked by a red +, the initial parameters by a green +. The misfit contours are normalized such that a value of 1 represents the 95% confidence interval.**

2.5. Amplitude vs. CO_2 layer thickness

The correlation between amplitude and CO_2 layer thickness can be further investigated with a 'plume' shaped model. For this model, the distribution of CO_2 is modelled as a plume, with a thickness of 15m in the center, tapering off uniformly to zero thickness at 200m from the center. Sources in this model were activated across the surface, generating a plane wave. In effect, this setup generates waves with normal incidence angle travelling through every point of the variable thickness plume. This allows us to observe the amplitude of reflection from different thicknesses of CO_2. I consider two models, where the velocity decreases caused by the CO_2 are 400 and 200ms^{-1}. The changes in amplitude as a function of plume thickness are plotted in Figure 18 for both models.

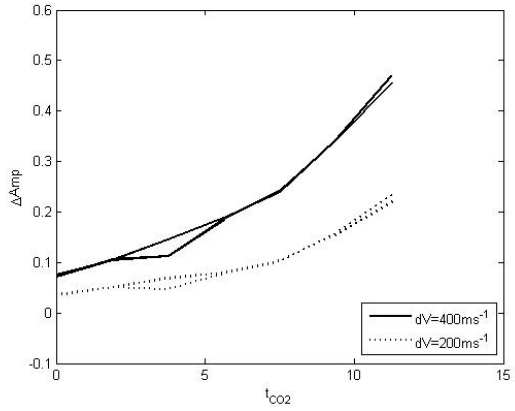

Figure 18: Change in amplitude of the reservoir reflection as a function of CO_2 thickness. Reflection amplitude increases with increasing CO_2 thickness and with larger velocity changes.

Figure 18 shows that reflection amplitude increases with increasing thickness of the CO_2 layer, and is also larger when the velocity change during CO_2 substitution is larger. The repeatability of the 4-D survey at CO_2SINK will be determined by variations in source and receiver locations, changes in near surface conditions, and by noise in the subsurface. Movement of remnant gas in the upper Jurassic gas-storage reservoir may also affect the repeatability. It is not the purpose of this report to assess the likely repeatability. However, assuming that the minimum detectable amplitude change decreases with increasing repeatability, it is clear that, whatever the repeatability may be, there will be a minimum thickness of CO_2 below which it will be undetectable. Improving the repeatability will mean that we can detect thinner layers. However, as discussed above, it will be difficult to reliably invert amplitude changes for velocity changes and layer thicknesses.

3. DISCUSSION

3.1. Quantitative estimates of CO2 distribution

There are two principal aims when monitoring CCS using 4-D seismics. The first is to identify regions where the injected CO_2 has migrated. The second is to make quantitative estimates about the amount of CO_2 in these regions. We have seen above that substitution of CO_2 for brine in the sandstone channels will produce measurable amplitude changes. This suggests that 4-D seismics will be able to detect areas where CO_2 has migrated, so long as the velocity change and layer thickness are of a sufficient magnitude, which will be determined by the repeatability. However, it does not appear possible to invert time-lapse observations for layer thicknesses and velocity changes. This means that the seismic response can be considered as a binary response, giving a yes-no answer to the question 'has the presence of CO_2 produced a velocity change?' but not allowing the computation of the amount of CO_2 present.

Gassmann substitution predicts that P-wave velocities are highly sensitive to the presence of compressible fluids such as CO_2, even in small amounts. It also predicts that, beyond a saturation of approximately 10%, the velocity is not sensitive to further increases. This means that it is impossible to differentiate seismically between areas saturated with 10% and 90% CO_2. For this reason, the binary seismic response to CO_2 substitution, where it is not possible to extract the CO_2 saturation, is not a new idea. However, my reasoning to arrive at this inference follows a different line than previous authors. This work goes one step further – the geometry and properties of the channels in the Stuttgart Formation are such that it may not be possible even to compute the magnitude of velocity change (from which saturation could be inferred) nor the thickness of the layer in which change has occurred. We can merely infer that a velocity change has occurred. Of course, even if a velocity change could be computed for the Ketzin case, computing the saturation from this velocity change would still encounter the same problem.

Perhaps the best way to make quantitative estimates of the CO_2 distribution in the reservoir would be to use the areal extent of the CO_2 plume, if it can be observed using seismics, to improve and constrain the fluid flow models that simulate the injection. This has proved the most successful method for generating quantitative estimates of CO_2 distribution at Weyburn (Wilson et al. 2004).

3.2. Migration of gas in the Jurassic reservoir

Above the target Stuttgart Formation lies the Jurassic reservoir that has been used in the past for gas storage. There is still remnant gas left in this reservoir, and its movements and location are not well known. This presents a potential issue in that movements of the remnant gas in the Jurassic reservoir could mask the 4-D seismic changes from the Stuttgart Formation. This must be kept in mind when processing the 4-D data. In the Wesser Formation overlying the Stuttgart Formation is a very strong reflection caused by the presence of a 20m thick anhydrite layer. This may be a useful marker, as it also lies below the Jurassic gas storage reservoir. Therefore, any changes caused by movement of gas in the upper reservoir would influence the arrival time and amplitude of this strong reflector as much as it would the reflections from the Stuttgart Formation. Therefore, when looking for the signal from CO_2 migration, it may potentially be a better option to consider the time shifts between the anhydrite and Stuttgart Formation rather than between the surface and the Stuttgart Formation, and the amplitude changes from the Stuttgart reflections as a fraction of the changes in amplitude of the anhydrite reflection, as this would remove the effects of remnant gas movement in the upper layers of the system.

3.3. Detection of CO2 without time-lapse information

In Autumn 2009 it is planned to conduct a 2-D survey around the injection site. There has been no base-line survey with which to compare amplitude or travel-time shifts. Without this information it will be difficult to disentangle the changes induced by CO_2 substitution from natural spatial variations in rock properties. However, this modelling study indicates that channels containing layers of CO_2 should have a higher amplitude reflection than channels containing brine. Channels have been identified during the baseline 3-D survey (Juhlin et al. 2007; Kazemeini et al. 2009), albeit with reflections that are difficult to observe above the noise levels without spectral decomposition (Kazemeini et al. 2009) or amplitude summation (Juhlin et al. 2007). If CO_2 substitution serves to increase the amplitudes reflected from these channels, then the Autumn 2009 2-D survey should have a better chance of identifying the geometry of the channels around the injection well.

4. CONCLUSIONS

Previous work assessing the feasibility of CO_2 detection using 4-D seismics at Ketzin has modelled the reservoir as a homogenous 80m thick sand body that becomes fully-saturated by CO_2. In reality, flow in the reservoir is controlled by the presence of channels, and flow simulations suggest that CO_2 will only be present in thin layers migrating along the top of the channels. In this work I develop simple models of thin channels with a thickness close to the tuning thickness in order to simulate the seismic response before and after the migration of CO_2 layers through these channels. These models show that reflection amplitudes will increase with the presence of CO_2. Therefore this change can be used to indicate the presence of CO_2. I then attempted to invert the forward modelled data for quantitative estimates of layer thickness and velocity change. However, this was not possible as there were trade-offs between dV and t_{CO2}. This suggests that seismic observations alone will not be sufficient to determine quantitatively the distribution of CO_2 through the reservoir.

4.1. Future work

The seismic response is quite sensitive to the initial, brine-saturated velocities of the sand and mud. These values have not been that well constrained. 3 differing velocity models have now been used for CO_2SINK by 3 different authors. If the baseline velocities are better understood, then we might be able to gain a more accurate estimation of the seismic response upon CO_2 saturation.

The data from the Autumn 2-D survey are expected by early 2010. The results from this survey should give us a much better indication of whether it is possible to detect the presence of the channels that are affecting the migration of the injected CO_2.

REFERENCES

[1] Arts, R., O. Eiken, A. Chadwick, P. Zweigel, L. van der Meer and B. Zinszner, 2004. Monitoring of CO_2 injected at Sleipner using time-lapse seismic data. Energy 29, 1383-1392.

[2] Chadwick, R.A., D. Noy, R. Arts and O. Eiken, 2009. Latest time-lapse seismic data from Sleipner yield new insights into CO_2 plume development. Energy Procedia, 2103-2110.

[3] Förster, A., B. Norden, K. Zinck-Jørgensen, P. Frykman, J. Kulenkampff, E. Spangenberg, J. Erzinger, M. Zimmer, J. Kopp, G. Borm, C. Juhlin, C. Cosma, S. Hurter, 2006. Baseline characterization of the CO2SINK geological storage site at Ketzin, Germany. Environmental Geosciences 13, 145-161.

[4] Ghaderi, A. and M. Landrø, 2009. Estimation of thickness and velocity changes of injected carbon dioxide layers from prestack time-lapse seismic data. Geophysics 74 (2), O17-O28.

[5] Ikelle, L.T. and L. Amundsen, 2005. Introduction to Petroleum Seismology. Society of Exploration Geophysicists, Tulsa, USA.

[6] Juhlin, C. and R. Young, 1993. Implications of thin layers for amplitude variation with offset (AVO) studies. Geophysics 58 (8), 1200-1204

[7] Juhlin, C., R. Giese, K. Zinck-Jørgensen, C. Cosma, S.H. Kazemeini, N. Juhojuntti, S. Lüth, B. Norden and A. Förster, 2007. 3D baseline seismics at Ketzin, Germany: The CO2SINK project. Geophysics 72 (5), B121-B132.

[8] Kallweit, R.S. and L.C. Wood, 1982. The limits of resolution of zero-phase wavelets. Geophysics 47 (7), 1035-1046.

[9] Kazemeini, S.H, 2009. Seismic investigations at the Ketzin CO_2 injection site, Germany: Applications to subsurface feature mapping and CO_2 seismic response modeling. Ph.D Thesis, Uppsala University, Sweden.

[10] Kazemeini, S.H., C. Juhlin, K. Zinck-Jørgensen and B. Norden, 2009. Application of the continuous wavelet transform on seismic data for mapping of channel deposits and gas detection at the CO2SINK site, Ketzin, Germany. Geophysical Properties 57, 111-123

[11] Oates, S. and A. Garnett, 2005. Note on Gassmann CO_2 fluid substitution scenarios for CO_2SINK project. Internal Shell report.

[12] Oates, S. and A. Garnett, 2006. Note on full waveform modelling of CO_2 flood time lapse seismic response for CO_2SINK project. Internal Shell report

[13] Verdon, J.P., D.A. Angus, J-M. Kendall and S.A. Hall, 2008. The effects of microstructure and nonlinear stress on anisotropic seismic velocities. Geophysics 73(4), D41-D51.

[14] Wilson, M., M. Monea, S. Whittaker, D. White, D. Law and R. Chalaturnyk, 2004. IEA GHG Weyburn CO_2 Monitoring and Storage Project Summary Report 2000-2004. PTRC. Available online at http://www.ptrc.ca/siteimages/Summary_Report_2000_2004.pdf

APPENDIX 1. GEOMECHANICAL MODELING AND SURFACE UPLIFT

A1.1. Summary

The operators of CO_2SINK plan to use satellite techniques to image surface uplift induced by CO_2 injection. It is of interest to develop models to predict how much uplift to expect at Ketzin. In this study I develop several simple geomechanical models in order to predict the magnitude and geometry of the uplift footprint. I examine the sensitivity of the uplift to material properties of the reservoir, and to the magnitude and the shape of the pressure plume in the reservoir. I show that uplift magnitudes are likely to be of a detectable magnitude, but that plausible models can be generated that have very low rates of uplift. I also show that the shape of the uplift footprint should assist in the identification of channels that are believed to modify the pressure plume in the reservoir.

A1.2. Introduction

Satellite monitoring of surface uplift has been used with great success at the B.P. operated In Salah CCS project. Surface uplift of ~4mm/year has been observed above the 3 injection wells, whilst subsidence has been observed above the main producing area of the reservoir. The desert surrounding In Salah is the perfect environment for deploying satellite techniques, meaning that the quality of data is good, with the uplift footprint well imaged (Vasco et al. 2008). Indeed, it has been argued that the presence of faults in or near the reservoir can be inferred from the uplift geometry, although this remains an issue of some debate.

At Ketzin, the farmland that surrounds the injection site is not such a good environment for performing satellite techniques, as permanent scatterers must be used. BGRM have conducted a feasibility study for the use of satellite PSI interferometry techniques at CO_2SINK. They have determined that there are sufficient permanent reflectors distributed around the injection site. Using data collected prior to injection, when there was no activity at the site, they have calculated that the maximum noise levels are ~3mm of uplift/subsidence per year. Deformation rates larger than this will therefore be detectable using this technique. However, as far as the author is aware, no work has been undertaken to use geomechanics to model the surface uplift as a result of injection.

A1.3. Fluid-flow Simulation

In order to model the geomechanical response to injection, it is first necessary to model the pressure changes induced by injection. This work has been conducted by M. Wellings *(pers. comm. 2009)* using Shell's in-house *MoReS* software. The model consists of the reservoir layer, which is 80m thick, with a constant dip to the south of 3 degrees. The majority of the reservoir consists of low quality floodplain deposits, but at the top of the reservoir is a higher quality channel that is 20m thick and 420m wide, striking N-S. This channel has the same porosity as the floodplain deposits, but twice the permeability. CO_2 is injected at the centre of this channel for a period of 1 year at a rate that matches that used at CO_2SINK.The model is depicted in Figure A1.1, and parameterized in Table A1.1. Only half of the model is actually computed, with symmetry arguments used to complete the simulation.

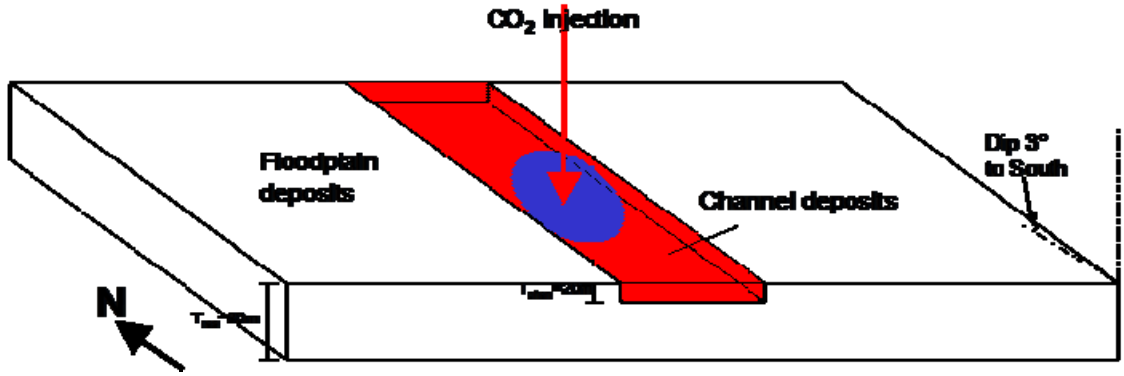

Figure A1.1: Schematic representation of the Stuttgart Formation at Ketzin, showing the key features included in the geomechanical modelling.

Table A1.1: Parameters used for the reservoir flow simulation (M. Wellings, pers. comm., 2009).

Parameter	Floodplain	Channel
Thickness	80m	20m
Width	14km	420m
Porosity	0.25	0.25
Permeability	0.05D	0.1D

The pressures computed can be input directly into the geomechanical simulation. The pressure field generated by this model is quite axisymmetric in shape (Figure A1.2). An issue at CO_2SINK that is as yet unresolved is whether the channels present 'no-flow' boundaries? Whether all of the CO_2, and all of the pressure increases, are restricted to the channels, or whether there are good flow connections through the floodplain deposits, as in the flow model discussed above? Therefore, it is of interest to compare the uplift generated by this axisymmetric pressure field to the uplift that would be generated if the pressure increases were confined to the channel. There is no reservoir flow model available that has this characteristic, so in order to generate an appropriate model, I created an artificial scenario where the pressure increases in the channel are the same as for the axisymmetric case, but outside the channel the pressure remains unchanged. The pressure fields at the end of injection for both cases are shown in Figures A1.2 and Figure A1.3.

A1.4. Geomechanical Model

In order to model the surface uplift, a 3-D geomechanical model was developed using Shell's in-house *Geomec* software. The model developed consists of several layers, listed in Table A1.2. The overburden at Ketzin is dominated by the presence of a stiff anhydrite layer. This layer is included specifically in our model. The layers above the anhydrite are modeled as uniform. The Triassic rocks below the anhydrite, which contain the reservoir, sideburden and immediate overburden, are also considered uniform. There are few material properties available for the rocks overlying the CO_2SINK reservoir, so approximate values have been used. For the cap-rock, elastic properties have been measured by Mutschler et al. (2009). However, they find an order of magnitude variation in Young's modulus, between 0.8-10GPa, depending on the sample size used.

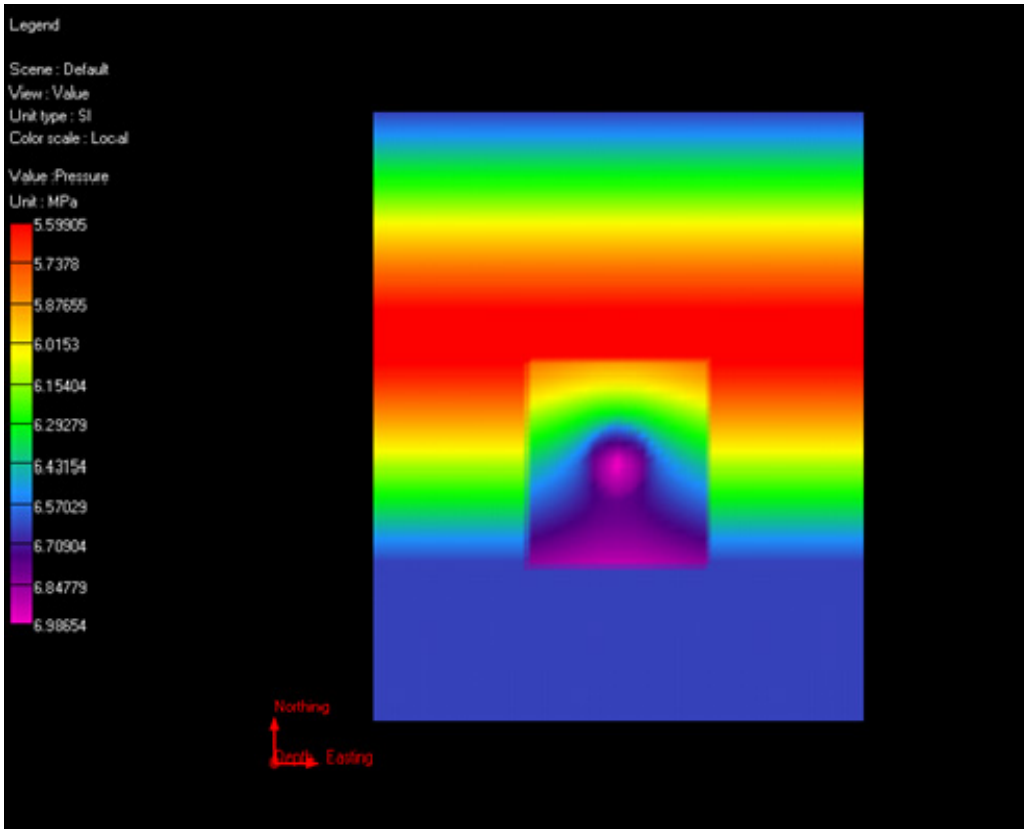

Figure A1.2: **Map view of the pressure field generated by the reservoir flow model at the end of the injection period.**

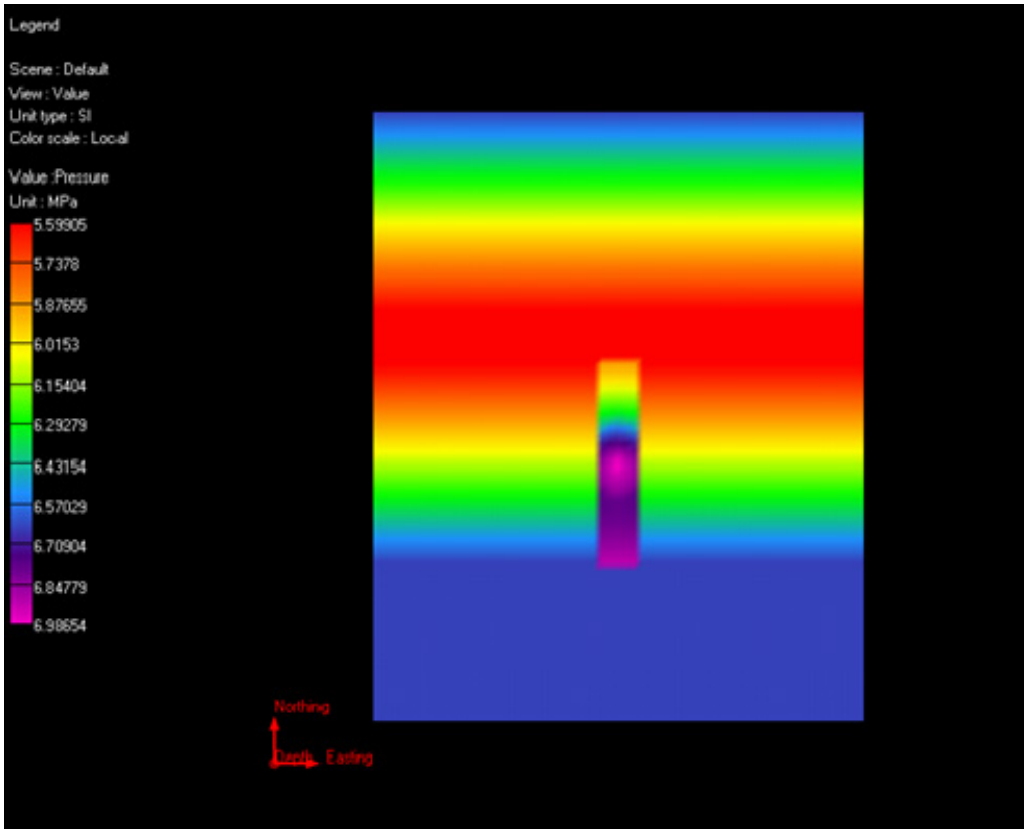

Figure A1.3: **Map of the pressure field at the end of injection, where pressure changes have been artificially limited to the channel deposits.**

Table A1.2: Layers present in the geomechanical model.

		Young's Modulus	Poisson's Ratio	Thickness
Overburden		1Gpa	0.2	389-435m
Anhydrite		56GPa	0.2	20m
Triassic:	Overburden	See Table A1.3	0.25	80-85m
	Reservoir	See Table A1.3	0.25	80m
	Underburden	See Table A1.3	0.25	143-234m

Four separate models will be presented in this report. I will vary the material properties of the rocks in and around the reservoir, and vary the pressure field between axisymmetric (model A) pressure increases and pressure increases in the channel only (models B-D). I also consider a case where the pressure increases have been doubled artificially (model C).

Table A1.3: Material properties and pressure fields that are varied between the models.

Model	Young's Modulus	Poisson's Ratio	Pressure field
A	5GPa	0.25	Axisymmetric
B	5GPa	0.25	Channel only
C	5GPa	0.25	Channel, dP is doubled
D	2GPa	0.25	Channel only

The model geometry is shown in Figure A1.4 in N-S cross-section. The gentle dips of the Ketzin anticline are modelled, with a dip of 3 degrees at the reservoir depth, reducing to 1.5 degrees in the anhydrite. The model is invariant in the W-E direction. The model extends a total of 5.39km in the N-S direction, and 4.34km in the E-W direction, with a uniform grid spacing of 70m. The rocks of the reservoir and overburden are approximated as behaving in a linearly elastic manner.

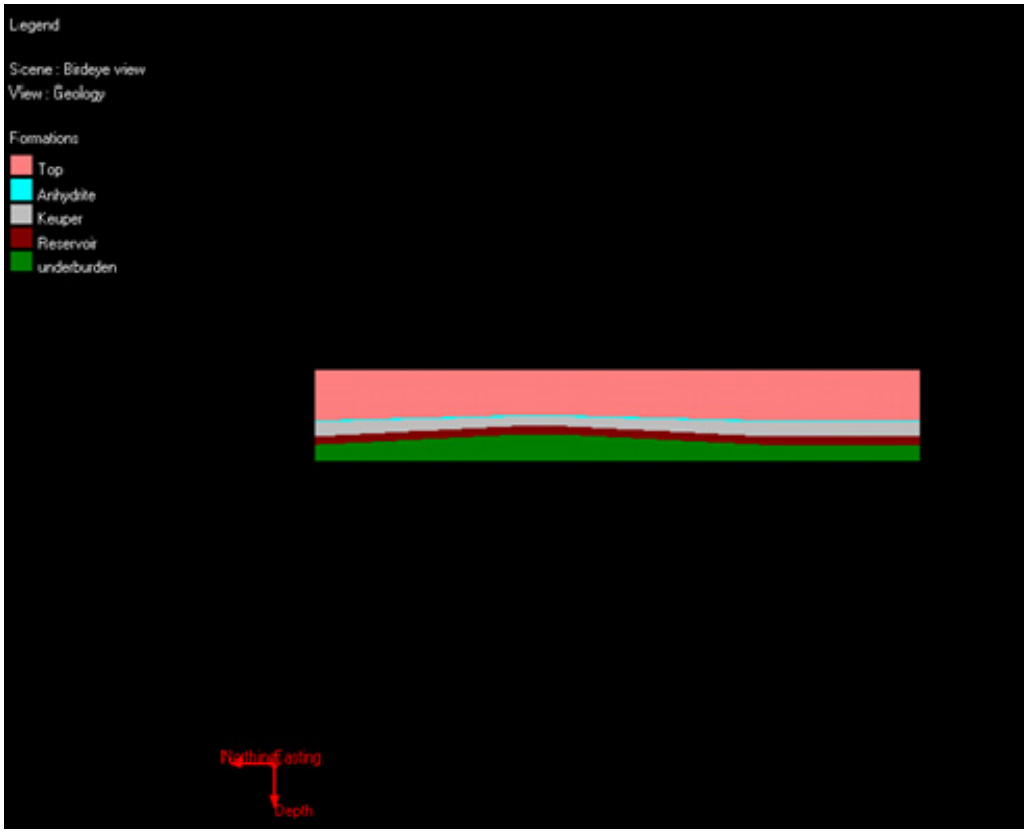

Figure A1.4: N-S cross-section through the Ketzin reservoir model. The material parameters foe the layers are given in Table A1.3. The model does not vary in the W-E direction.

A1.5. Results:

The uplift across the model is provided as an output from the *Geomec* model. A map view of surface uplift for Model A is plotted in Figure A1.5. East-West cross-sections of the uplift profiles through the injection well are plotted in Figure A1.6 for all models. The preliminary work from BGRM suggests that uplift larger than 3mm will be observable – 3 of the 4 models predict uplift larger than this amount. Model A, with an axisymmetric pressure increase, predicts a larger amount of uplift than Model B, which has the same material properties and pressure increase, excepting that Model B has pressure increases inside the channel only. The uplift in Model A is larger both in amplitude and wavelength than Model B. The cause for this almost doubling of uplift amplitude is due to the amount of stress arching that can occur – this will be discussed further below. The amount of uplift appears to be more sensitive to the magnitude of the pressure increase than the material properties, as doubling the pressure increase (Model C) generates 3mm more uplift than reducing by 2.5 times the Young's Modulus (Model D).

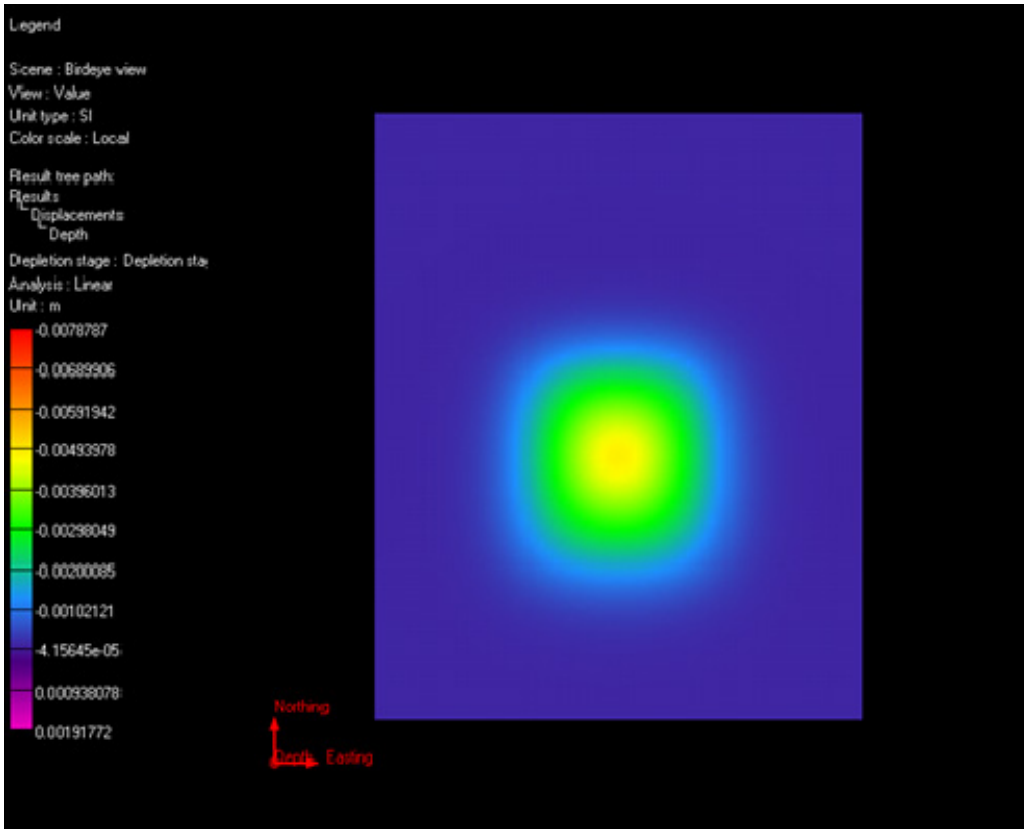

Figure A1.5: Map view of surface uplift for Model A.

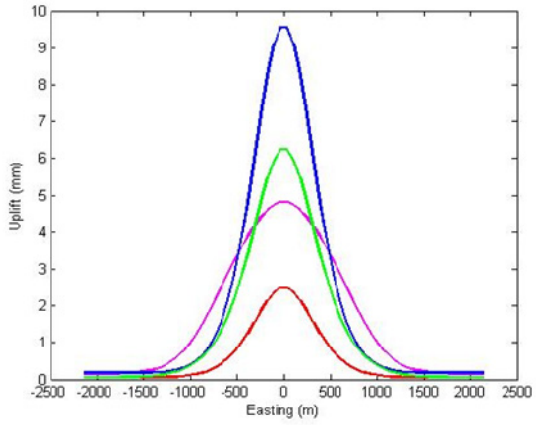

Figure A1.6: W-E cross-sections of the uplift through the injection well (at 0m). The lines correspond to models A=magenta, B=red, C=blue and D=green.

A1.6. Detectability of Uplift

The baseline study conducted by BGRM has indicated that the noise levels for PSI interferometry are ~3mm. The 3 of the 4 models indicate a maximum uplift rate larger than this value. However, the uplift rates for Model B may well be undetectable. Model B has pressure increases in the channel only, but material properties that are appropriate, and the pressure increases have not been exaggerated (as in Model C). Therefore, I must conclude that although some models to indicate detectable uplift, there are perfectly plausible geomechanical models that do not. The two key dependent parameters are the Young's modulus of the reservoir material (which is not well constrained) and the lateral

extent of the pressure increase, which controls the amount of stress arching and therefore uplift. This is also poorly understood.

A1.6.1. Wavelength of Uplift

If uplift can be detected, it will be of interest to consider the lateral extent of this uplift. If elevated pressures are contained within the higher permeability channels, then the geomechanical models suggest that surface deformation will be narrower and more linear, tracking the path of the channel in the subsurface. This would be a crucial observation to make at CO_2SINK, as thus far seismic techniques have struggled to resolve the geometry of channels in the Stuttgart reservoir (e.g., Juhlin et al. 2007). However, with only a few permanent reflectors around the injection site, it may be too big of an ask to constrain the geometry of the uplift well enough to make this distinction.

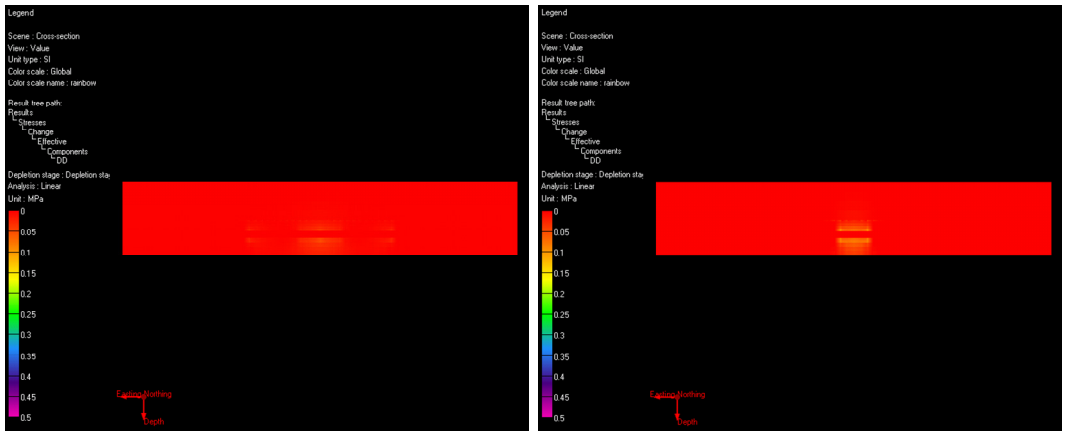

Figure A1.7: Cross section showing changes in vertical stress for Models A and B. These models have the same material properties and pressure changes, excepting that in Model B the pressure changes are restricted to a thin channel. In Model A, the loading is mostly supported in the reservoir (not plotted), meaning that there is little stress evolution in the overburden. In contrast, as Model B has a smaller lateral extent, stress arching can occur, resulting in compaction (stress increase) in the overburden. The effect of stress arching is to reduce the magnitude of surface uplift.

A1.6.2. Stress Arching

It is interesting to note the differences in uplift between Models A and B. These models have the same material properties and the same magnitude of pressure changes. The difference is that in Model B the pressure increases are limited to the channel. As a result, the uplift rates are almost doubled for Model A compared to B. This demonstrates the importance of stress arching in controlling uplift rates. It has been shown (e.g., Segura et al., 2008) that, given identical material properties, stress-arching effects will be larger for reservoirs with a smaller aspect ratio (width/thickness). Verdon et al. (2008) show that it is the smallest lateral dimension that controls whether stress arching can occur. Therefore, I anticipate greater stress arching over Model B, with the long, thin, channel reservoir, than over Model A, with the more extensive pressure increases. Figure A1.7 shows cross sections through the centre of both these models, showing the change in effective vertical stress (decreases in effective stress inside the reservoir caused by pore pressure increases are blanked out here). Model A shows very little stress change outside of the reservoir,

indicating that there is no stress arching occurring. In contrast, Model B shows an increase in effective stress above the reservoir, implying compression as the reservoir pushes upwards, but the overburden is held in place by the sideburden. The net result is that rather than being uplifted, the overburden is compressed.

A1.7. Conclusions:

Surface deformation will be monitored at CO_2SINK using satellite methods. This work presents some simple geomechanical modelling to assess the likely magnitudes of uplift to be expected at Ketzin. A fluid flow model has been used to provide the loading for a simple, layered geomechanical model representing the Ketzin anticline. I find that uplift rates are dependent on the material properties of the reservoir, the magnitude of the pressure increase, and the lateral extent of the region of pressure increase. Of the models generated, most predict uplift rates of a detectable magnitude. However, plausible models can be constructed which generate uplift rates below what is likely to be detectable at Ketzin.

A1.8. Future Work:

This work represents a simple modelling experiment to determine whether detectable amounts of uplift are likely above the CO_2SINK reservoir. As yet, the mechanical properties of the overburden at Ketzin have not been well constrained. Although these models are not very sensitive to overburden properties, determining these properties would improve the accuracy of surface uplift models. This may also allow more complete behaviour to be modelled, including plastic failure and visco-elastic flow. This information could be combined with the available data giving the actual geometry of the Ketzin anticline to provide a much more complete geomechanical model. Should uplift be detected at CO_2SINK, the it is likely that this would be necessary to invert the surface deformation observations for deformation and the stress/pressure fields at reservoir depths.

A1.9. References

Mutschler, T., T. Triantafyllidis, K. Balthasar, 2008. Geotechnical investigations of cap rocks above CO_2 reservoirs. Energy Procedia 1(1), 3375-3382.

Segura, J.M., S. Skachkov, Q.J. Fisher, 2008. Controls on reservoir stress path. EAGE Annual Meeting, Rome, Expanded Abstracts, P128.

Vasco, D.W., A. Ferretti, F. Novali, 2008. Reservoir monitoring and characterization using satellite geodetic data: Interferometric synthetic aperture radar observations from the Krechba field, Algeria. Geophysics 73(6), WA113-WA122.

Verdon, J.P., D.A. Angus, J-M. Kendall, J. Segura, S. Skachkov, Q.J. Fisher, 2008. The effects of geomechanical deformation on seismic monitoring of CO2 sequestration. SEG Annual Meeting, Las Vegas, Expanded Abstracts 27, 2869-2873.

DISTRIBUTION LIST

Paper copy distribution

OU	*Recipient*	*Ref.ind.*	*No. of copies*
SIEP Rijswijk	Library	EPT-IT-SI	1
SIEP Rijswijk	N. Hodgson	EPT-RHS	1
SIEP Rijswijk	F. de Bree	EPT-RHS	1
SIEP Rijswijk	F. Kraaijeveld	EPT-RHS	1
SIEP Rijswijk	P. Fokker	EPT-RHS	1
SIEP Rijswijk	S. Grandi	EPT-RHS	1
SIEP Rijswijk	C. Otto	EPT-RXX	1
SIEP Rijswijk	M. Welling	EPT-RXX	1
SIEP Rijswijk	R. Wentinck	EPT-RXX	1
SIEP Rijswijk	S. Oates	EPT-RHS	1
SIEP Rijswijk	X. Campman	EPT-RXX	6
SIEP Rijswijk	A. Busch	EPT-RXX	1
SIEP Rijswijk	H. Klemm	EPT-RHS	1